Dark Characterization of Ti/Al LEKIDs for the Search of Axions in the W-Band

Victor Rollano, Alejandro Pascual Laguna, David Rodriguez, Martino Calvo, Maria Teresa Magaz, Daniel Granados, Alessandro Monfardini, and Alicia Gomez

***Abstract*—In this article, we report the electrical (dark) characterization of lumped-element kinetic inductance detectors (LEKIDs) fabricated from a titanium/aluminum bilayer and designed for broadband absorption in the W-band (75–110 GHz). These detectors are prototypes for future quantum chromodynamics axion search experiments within the Canfranc axion detection experiment (CADEx), which demand sub-$10^{-19}\mathrm{W}/\sqrt{\mathrm{Hz}}$ sensitivities under low optical backgrounds. We combine a Mattis–Bardeen analysis to the temperature dependence of the detector parameters with noise spectroscopy to determine the electrical noise equivalent power (NEP). The minimum measured value for the electrical NEP is $\sim 3 \times 10^{-19}\mathrm{W}/\sqrt{\mathrm{Hz}}$. Across the measured temperature range, we find that quasiparticle lifetime deviates from the expected BCS recombination law. Our analysis suggests that nonequilibrium relaxation is governed by spatial inhomogeneities in the superconducting gap and phonon diffusion effects. This work sets the road-map to achieve suitable and ultra-sensitive detectors in the W-band for dark matter axion search experiments.**

***Index Terms*—Absorber, axions, microwave kinetic inductance detectors (MKID), titanium/aluminum (Ti/Al).**

I. Introduction

MICROWAVE kinetic inductance detectors (MKIDs) have emerged as a leading technology for large-format, ultralow-noise detection at millimeter and submillimeter wavelengths. Their inherent multiplexability, simple planar fabrication, and straightforward cryogenic integration make them attractive for astrophysical and laboratory instruments targeting background-limited performance. MKIDs are now deployed in several (sub)millimeter cameras and spectrometers, including NIKA2 [1], CONCERTO [2], and DESHIMA [3]. Recently, MKIDs have been confirmed as the selected type of detectors for the PRIMA space telescope of NASA, ratifying its status as a leading detector technology [4].

Within the MKID family, lumped-element kinetic inductance detectors (KIDs) (LEKIDs) offer flexible impedance and absorber design, advantageous for broadband operation in the W-band (75–110 GHz). We have developed a prototype array of LEKIDs intended for the Canfranc axion detection experiment (CADEx) [5], which aims to search for axion dark-matter signatures (via the Primakoff conversion/decay channel) in the 330–460 μeV mass range, corresponding to W-band photons. As incoherent (direct) detectors, MKIDs are not limited by the quantum noise like coherent receivers are [6]. This means that, for a given detection bandwidth $\Delta\nu$, direct detectors like MKIDs can match or even beat the sensitivity of coherent detectors, which makes them extremely attractive for dark matter detection experiments.

The figure of merit for a power-integrating direct detector is the noise equivalent power (NEP), defined as the input-referred power spectral density that yields a signal-to-noise-ratio SNR $=$ 1 in a 1Hz output bandwidth. In most applications, the NEP is measured under illumination, ideally being limited by photon noise (shot and, when relevant, bunching), which can mask the detector's intrinsic performance. In this sense, CADEx requires an NEP as low as $\sim 10^{-20}\,\mathrm{W}/\sqrt{\mathrm{Hz}}$.

This work focuses on the electrical characterization of the CADEx camera prototype in dark conditions, to determine the device electrical NEP, which imposes a lower bound on the optical NEP. The rest of this article is organized as follows. Section II presents the fabricated titanium/aluminum (Ti/Al) LEKIDs and reviews the experimental details. In Section III, the radio-frequency (RF) characterization results and their analysis is presented; describing the quasiparticle electrodynamics and reporting the dark electrical NEP. Section IV presents the discussion. Finally, Section V concludes this article and proposes improvements for future implementations based on these findings.

II. Experimental Section

The device studied in this work consists of nine LEKIDs organized in a 3×3 array, all of them coupled to a microstrip transmission line that serves as readout line. Each detector has a different resonance frequency, with adequate frequency spacing (> 3 MHz) to permit multiplexed readout without crosstalk [7]. The sample has been fabricated using a Ti/Al bilayer deposited onto a 275μm-thick high-resistivity ($\rho > 1\,\mathrm{k}\Omega \cdot \mathrm{cm}$) silicon (Si)

Received 26 September 2025; revised 14 January 2026; accepted 5 February 2026. Date of publication 23 February 2026; date of current version 3 March 2026. This work was supported in part by EU "NextGenerationEU"/PRTR and in part by "ERDF A way of making Europe" under Grant PID2022-137779OB-C41, Grant PID2022-137779OB-C42, and Grant JDC2023-051842-I. *(Corresponding authors: Victor Rollano; Alicia Gomez.)*

Victor Rollano, Alejandro Pascual Laguna, David Rodriguez, Maria Teresa Magaz, and Alicia Gomez are with the Centro de Astrobiología (CSIC-INTA), 28850 Torrejón de Ardoz, Spain (e-mail: vrollano@cab.inta-csic.es; agomez@cab.inta-csic.es).

Daniel Granados is with the Instituto Madrileño de Estudios Avanzados en Nanociencia (IMDEA Nanociencia), 28049 Madrid, Spain.

Martino Calvo and Alessandro Monfardini are with the Institut Néel, CNRS and Université Grenoble Alpes, 38042 Grenoble, France.

Color versions of one or more figures in this article are available at https://doi.org/10.1109/TASC.2026.3664493.

Digital Object Identifier 10.1109/TASC.2026.3664493

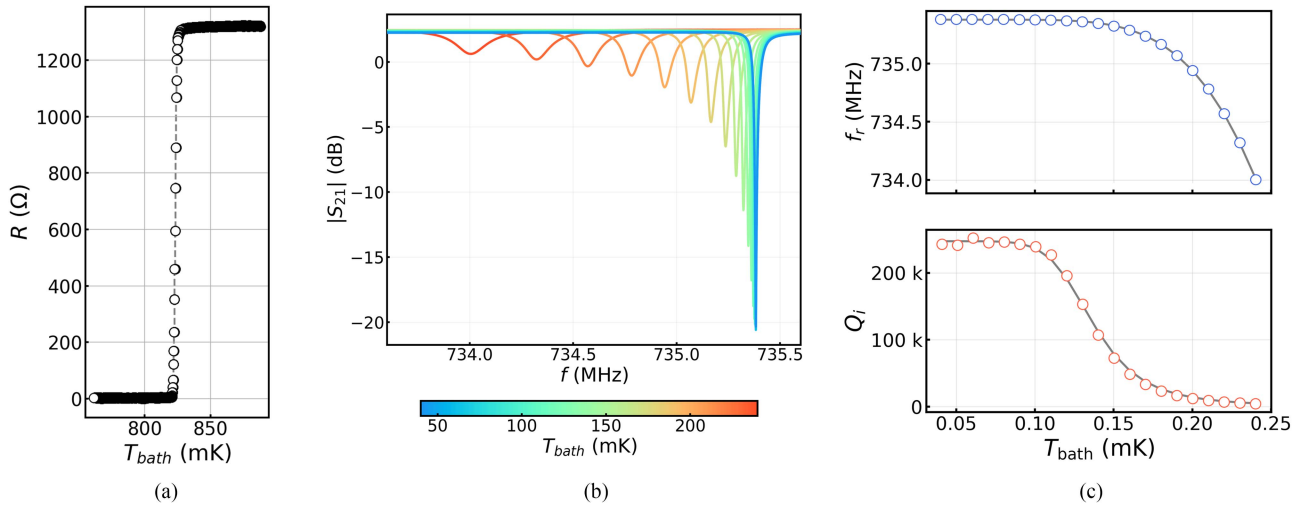

Fig. 1. (a) Resistance as a function of temperature for a meander of 10 μm width and 10.785 mm long measured with a DC current. (b) Transmission amplitude as a function of readout frequency for various bath temperatures between 40 and 240 mK. The microwave readout power at the chip level is fixed at –90 dBm. (c) Extracted resonance frequency (top) and internal quality factor (bottom) as functions of bath temperature. Gray solid lines represent fits of the experimental data using the MB model.

substrate. The substrate thickness is chosen to approximate a quarter-wave optical thickness near 90 GHz, at the center of the W-band. Native Si oxide is removed in a 1% hydrofluoric acid bath; within one minute the wafer is loaded into a confocal sputtering chamber with base pressure of $\sim 10^{-9}$ Torr. The Ti/Al stack consists of a 10 nm Ti base layer capped with a 20 nm Al layer. An additional 200 nm Al film is deposited on the backside of the wafer serving as both a reflective backshort and ground plane. During the metal deposition, the argon pressure is maintained at 10^{-3} Torr, reaching a target evaporation rate of 0.22 Å/s for Ti and 0.24 Å/s for Al. We performed the device patterning on a maskless laser-writer photolithography using AZnLOF 2070 negative photoresist. After developing the resist, the uncovered metal was removed using wet etching (90 s in Al80 for aluminum and 180 s in TBR19 for titanium). Then, the remaining resist is removed using an acetone and isopropanol rinse. Additional information on the detector design can be found elsewhere [7].

The electromagnetic response of the prototype has been characterized in a BlueFors LD250 dilution refrigerator. The device is mounted in a closed sample holder in thermal contact with the mixing chamber of the cryostat. The inner walls of the sample holder are painted with carbon-loaded epoxy and SiC grains, an absorber material, trying to maintain the darkest environment as possible. A homodyne IQ readout set up is employed to perform the RF measurements. A microwave signal generator provides a continuous-wave probe that is split by a power divider: one output serves as the local oscillator (LO) for an IQ mixer, while the other passes through a room-temperature variable attenuator (to set the input power) and then into the cryostat. The input coaxial line inside the refrigerator provides -40 dB of cold attenuation before the signal reaches the device. The transmitted signal is amplified at the 4 K stage by a low-noise amplifier with a noise temperature of $\sim$ 5K, and fed to the RF port of the in-phase (I) and quadrature (Q), IQ, mixer for homodyne demodulation using the common LO. The in-phase (I) and quadrature (Q) outputs are digitized using a National Instruments PXI-5922, operated typically at 1 MSa/s with an effective 22-b vertical resolution.

The choice of using a Ti/Al stack obeys the fact that the superconducting gap Δ imposes a detection frequency lower limit. Typical MKIDs fabricated from aluminum cannot detect photons below $2\,\Delta_{Al}/h \sim 90$ GHz. Adding a thin layer of titanium below the aluminum tends to lower Δ due to proximity effect, making the device suitable for the entire W-band [8]. As an initial characterization, the superconducting transition was determined by measuring the resistance of a Ti/Al meander as a function of temperature. Fig. 1(a) shows the DC measurement of the transition. The critical temperature, defined at $0.5R_n$, is 820 mK, with R_n being the resistance before the superconducting transition. Using the BCS relation $\Delta_0 = 1.764\,k_B T_c$, we obtain a zero-temperature superconducting gap of $\Delta_0 = 124.6\,\mu$eV. In the normal state, the bilayer exhibits a sheet resistance of $R_{s,\square} \approx 1.22\,\Omega/\text{sq}$. Within the BCS dirty-limit framework, the kinetic inductance per square can be estimated as $L_{k,\square} = \hbar R_{s,\square}/(\pi\Delta_0)$, yielding $L_{k,\square} \approx 2.02$ pH/$\square$.

III. Results

A. Superconducting Electrodynamics

We investigated the electrodynamics of the Ti/Al bilayer under dark, thermal-equilibrium conditions by monitoring the detector response versus bath temperature (T_{bath}). Fig. 1(b) shows the variation in the amplitude of transmission parameter $|S_{21}|$ as T_{bath} increases from 40 to 240 mK for one representative detector. The resonator was probed with a microwave readout signal of -90 dBm at the chip input (i.e., after accounting for the attenuation of the input line). This choice for the readout power is justified as it is the highest value that avoids nonlinear response. As the temperature rises, the resonance dip shifts to lower frequencies and broadens, reflecting the increase in kinetic inductance and in the losses of the Ti/Al bilayer.

The transmission data at each temperature were analyzed by fitting to the model described in [9]. From this analysis, we extracted the resonance frequency (f_r) and the internal quality factor (Q_i) as functions of temperature, as shown in Fig. 1(c). The same panel also includes fits to the Mattis–Bardeen (MB) model at low temperature, expressed as [10]

$$f_r(T) = f_r(0)\left[1 + \frac{\alpha}{2}\left(1 - \frac{S_2(0)}{S_2(T)}\right)\right] \tag{1}$$

and

$$Q_i^{-1}(T) = Q_{\text{sat}}^{-1} + \frac{2\alpha}{\pi}\frac{\Delta_0}{\Delta(T)}\frac{S_1(T)S_2(0)}{S_2(T)} \tag{2}$$

using $S_1(T)$ and $S_2(T)$ as defined in [11].

In this model, the kinetic-inductance fraction is defined as

$$\alpha \equiv \frac{L_k}{L_k + L_g} \tag{3}$$

where L_g is the geometric inductance of the resonator. The parameters $f_r(0)$ and Q_{sat} are the resonance frequency and the residual value of Q_i in the zero-temperature limit, where MB quasiparticle loss can be considered negligible. For temperatures well below T_c, the superconducting gap Δ is assumed to vary with temperature as [10]

$$\Delta(T) = \Delta_0\left[1 - \sqrt{\frac{2\pi k_B T}{\Delta_0}}e^{-\Delta_0/k_B T}\right]. \tag{4}$$

The fit to the resonance frequency as a function of temperature, as shown in Fig. 1(c), yields $\alpha = 0.34$, $\Delta_0 = 123.72\mu$eV (corresponding to $T_c \approx 814.7$mK), and $f_r(0) = 735.38$ MHz. The Δ_0 value obtained from both MB analysis and DC transport measurements are compatible, ensuring sensitivity to excitations above $\Delta_{\text{Ti/Al}}/h \sim 59$GHz, making this material suitable for detection in the entire W-band (75GHz − 110GHz). Best-fit parameters for $Q_i^{-1}(T)$ are $\alpha = 0.374$ and $Q_{\text{sat}} = 2.45 \times 10^5$, with the value Δ_0 being fixed from the resonance frequency fit.

We have compared the values obtained for α from the fitting analysis with the ones that can be computed from electromagnetic simulations of the resonator design using Sonnet [12]. The geometric inductance obtained from EM simulations is $L_g \approx 33$ nH. For an inductor of 9256 sq, the total kinetic inductance is $L_k \approx 19$ nH, yielding a kinetic fraction of $\alpha_{\text{sim}} \approx 0.37$.

B. Noise Spectra and Quasiparticle Dynamics

In this section, we present noise spectra analysis as a starting point to later characterize the sensitivity of the detectors. We acquired noise traces as a function of the temperature of the quasiparticle bath T_{bath}. Each trace is composed of 20 noise samples of 1 s sampled at 500 kSa/s. The microwave stimulus is set in the resonance frequency of the resonator at each value of T_{bath}. The readout power, as in the previous section, is maintained at −90 dBm.

The phase noise single-sided power spectral density $S_\theta(f)$ measured for several bath temperature values is shown in Fig. 2. At low temperatures, we observe a noise spectrum that presents two different roll-offs. The high frequency one corresponds to the electromagnetic energy decay of the resonant mode,

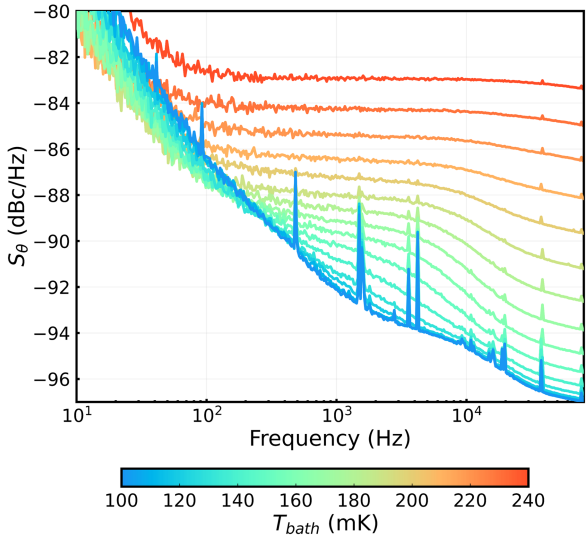

Fig. 2. Measured phase noise power spectral density as a function of audio frequency for a single detector measured at different bath temperatures between 40 and 240 mK, increasing from bottom to top. Microwave readout power is −90 dBm, while the frequency of the readout signal is fixed at the resonance frequency obtained from fitting each trace.

characterized by a decay rate $\kappa = f_r/(2Q_L)$. Here, Q_L is the loaded quality factor, which includes both the internal losses and the external coupling rate to the transmission line. Stepping down in frequency, we find a second roll-off, which we attribute to the quasiparticle generation–recombination (GR) processes. As temperature increases, the GR bandwidth upshifts toward higher frequencies and increases its noise level, a behavior expected from the GR kinetics [13]. At high temperatures, the GR roll-off hides the resonator bandwidth completely. Finally, the low-frequency band is dominated by a 1 over f slope.

The phase noise single-sided PSD due to the GR dynamics can be modeled as

$$S_\theta(f) = \frac{4N_{\text{qp}}\tau_{\text{qp}}}{1 + (2\pi f\tau_{\text{qp}})^2}\left(\frac{\delta\theta}{\delta N_{\text{qp}}}\right)^2 \tag{5}$$

where τ_{qp} is the GR characteristic time and N_{qp} is the mean quasiparticle number.

In Fig. 3(a), we show best-fit results for four representative phase noise spectra measured at 100, mK, 130, mK, 150, mK, and 170, mK. Each on-resonance spectrum has been baseline-corrected by subtracting the off-resonance spectrum, thereby removing the amplifier white-noise floor contribution. The model used to fit the phase noise consists on the Lorentzian shape from (5), with the addition of a $1/f$ contribution and another Lorentzian shape due to the resonator roll-off, with a characteristic time $\tau_{\text{res}} = 2\,\pi\kappa^{-1}$. The dash-dot curve in Fig. 3(a) represents the isolated GR component given by (5).

Fig. 3(b) depicts the obtained GR time as a function of temperature $\tau_{\text{qp}}(T)$. We first compare the extracted data against the Kaplan quasiparticle recombination model [14]

$$\tau_{\text{qp}}(T) = \frac{\tau_0}{\sqrt{\pi}}\left[\frac{k_B T_c}{2\Delta(T)}\right]^{5/2}\sqrt{\frac{T_c}{T}}e^{\Delta_0/k_B T} \tag{6}$$

using Δ_0 fixed by the measured critical temperature and the MB fits to $f_r(T)$ and $Q_i(T)$. With these inputs, the Kaplan

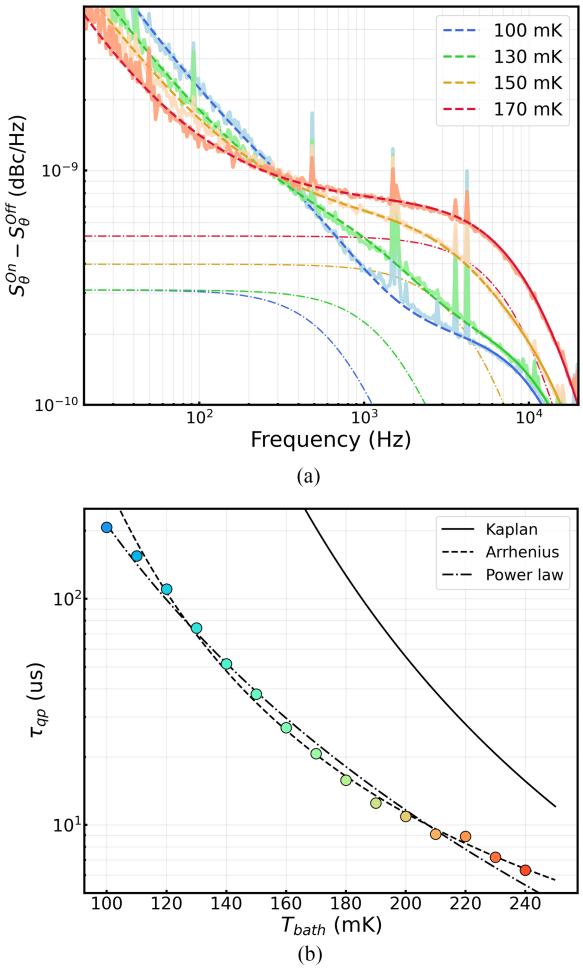

Fig. 3. (a) Fits of measured noise power spectral densities together with their corresponding roll-off components, shown for four representative bath temperatures (100 mK, 130 mK, 150 mK, and 170 mK). The fitting is performed using the model described in (5). Dashed lines indicate the full model fit, while dash-dot lines highlight the quasiparticle Lorentzian roll-off contribution. PSD curves are shown after subtraction of the off-resonance spectra, thereby removing the amplifier noise floor. (b) Quasiparticle recombination time as a function of bath temperature, extracted from the Lorentzian fits in the PSDs. Black solid, dashed, and dash-dotted curves represent the Kaplan, modified Arrhenius, and phonon–electron coupling models.

model does not describe the GR dynamics in the Ti/Al bilayer (see black solid line), even when using a phonon trapping factor $\tau_{qp}^* = \tau_{qp}(1+\beta)$ [15] that modifies the apparent quasiparticle lifetime. The gap needed to reproduce the kink observed in the measured τ_{qp} is too low to be fitted by the proximitized gap obtained from the measured superconducting transition. This may be indicative of some other processes affecting the quasiparticle kinetics in the detector and modifying the temperature dependence.

To extract physical information from these data, we have used the following two different phenomenological models.

1) We fitted the GR recombination time with a modified Arrhenius model

$$\tau_{qp} = \tau_0 \exp\left[m\Delta(T)/k_B T\right]. \tag{7}$$

The fit yields $m = 0.47$ and $\tau_0 = 388$ns. The result $m < 1$ can be interpreted as an effective activation energy below Δ_0 due to subgap states or gap spatial inhomogeneity associated with disorder or proximity effects in the bilayer [16], [17]. The resulting fit is plotted in Fig. 3(b) using a dashed black curve.

2) Exploring the possibility that the dominant energy dissipation mechanism is the electron–phonon coupling, which introduces a heavy dependence of τ_{qp} on temperature, we have also used a power-law to fit the data as [18], [19]

$$\tau_{qp} = AT^{-n}. \tag{8}$$

The fit using this model is shown in Fig. 3(b) with a dash-dot black line. The fit yields $n \approx 4.1$, typical of disordered superconductors [20], and $A \approx 1.37 \times 10^{-8} K \cdot s^{-4.1}$.

C. Dark Sensitivity

The phase response of the detector as a function of T_{bath} is presented in the top panel of Fig. 4(a). At each temperature, the complex transmission was digitized for 1 ms while applying a continuous probe tone, and after repeating 10 times, the digital reading was averaged. As in previous sections, the microwave power is maintained at -90dBm. Then, bath temperature is increased 1 mK and the complex trace is acquired again following the same procedure. Using four response points around each main bath temperature (stepped 1 mK), we extract the electrical phase responsivity $\delta\theta/\delta T_{bath}$ as the slope of the phase response, as pictured in Fig. 4(a). The obtained electrical phase responsivity is plotted in the bottom panel of Fig. 4(a).

From this, we obtain the dark electrical responsivity as

$$\frac{\delta\theta}{\delta P_{dark}} = \frac{\eta_{pb}\tau_{qp}(T)}{\Delta(T)} \frac{\delta\theta}{\delta N_{qp}} \tag{9}$$

where η_{pb} is the pair-breaking efficiency and N_{qp} is the mean quasiparticle number in thermal equilibrium. We related $\delta\theta/\delta N_{qp}$ to the measured $\delta\theta/\delta T_{bath}$ using

$$\frac{\delta\theta}{\delta N_{qp}} = \frac{\delta\theta}{\delta T_{bath}} \left(\frac{\delta N_{qp}}{\delta T_{bath}}\right)^{-1} \tag{10}$$

with $N_{qp}(T)$ given, for $T \ll T_c$, by the standard BCS low-temperature asymptotic expression

$$N_{qp}(T) = 2N_0 V \sqrt{2\pi k_B T \Delta(T)} e^{-\Delta(T)/k_B T} \tag{11}$$

where N_0 is the single-spin electronic density of states (DOS) at the Fermi level and V is the active superconducting volume (i.e., the inductor volume). We approximated the effective N_0 of the bilayer as the weighted average

$$N_0^{\text{eff}} = \frac{N_0^{\text{Al}} t_{\text{Al}} + N_0^{\text{Ti}} t_{\text{Ti}}}{t_{\text{Al}} + t_{\text{Ti}}} \tag{12}$$

where t_{Al} and t_{Ti} represent the thickness of the aluminum and titanium layers, respectively, and with $N_0^{\text{Al}} = 1.74 \times 10^{10} \mu\text{m}^{-3}\text{eV}^{-1}$ and $N_0^{\text{Ti}} = 4.1 \times 10^{10} \mu\text{m}^{-3}\text{eV}^{-1}$ [21].

We use $\Delta(T)$ obtained from the MB analysis of $f_r(T)$ and $Q_i(T)$ because the dark electrical responsivity is an equilibrium quantity that depends on the thermal quasiparticle population N_{qp}. The MB fit yields a self-consistent $\Delta(T)$ tied to the film's equilibrium electrodynamics. In contrast, the τ_{qp} analysis probes

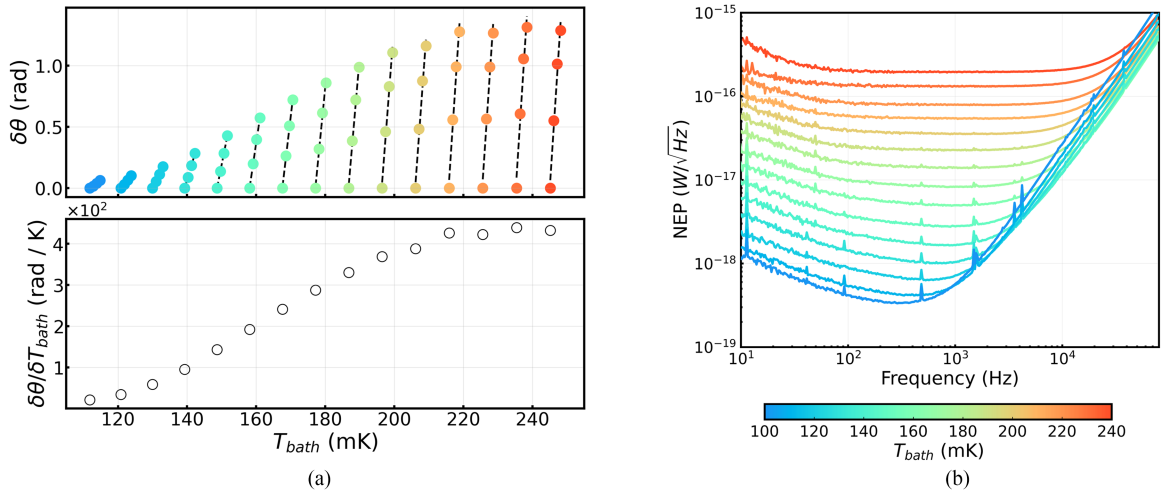

Fig. 4. (a) Phase response (top) and phase responsivity (bottom) as functions of bath temperature. Each phase response is referenced to the center of the corresponding resonance trace measured at the same temperature. (b) Measured electrical NEP in the resonator phase as a function of audio frequency for bath temperatures between 100 and 240 mK.

dynamics (small fluctuations δN around $N_{\rm qp}$) and can be influenced by nonequilibrium effects, such as readout power, phonon bottlenecking, and trapping. Using the MB-derived $\Delta(T)$ to compute $N_{\rm qp}(T)$ cleanly separates the equilibrium DOS (which sets the mean $N_{\rm qp}$) from the relaxation kinetics (which set $\tau_{\rm qp}$), avoiding biases from nonequilibrium corrections in the lifetime fit.

Finally, we obtain the dark electrical NEP as

$$\mathrm{NEP}_{\rm dark}(f) = \sqrt{S_\theta}\left(\frac{\delta\theta}{\delta P_{\rm dark}}\right)^{-1}\sqrt{1+(2\pi f\tau_{\rm qp})^2}. \quad (13)$$

The measured dark electrical NEP as a function of frequency for several values of the bath temperature from 100 to 240 mK is shown in Fig. 4(b). The NEPs are determined from the measured noise spectra and responsivities. We find that the best value of the electrical NEP, for a frequency of 200 Hz and $T_{\rm bath} = 100$ mK is $3 \times 10^{-19}\,\mathrm{W}/\sqrt{\mathrm{Hz}}$.

IV. Discussion

Our work shows that the Ti/Al bilayer low temperature physics in thermal equilibrium are well captured by the MB framework. The analysis of the $f_r(T)$ and $Q_i(T)$ yield a superconducting gap of $\Delta_0 \approx 124\,\mu$eV, a value consistent with the measured T_c. However, the quasiparticle recombination time extracted from GR roll-off in the PSDs deviates from the typical Kaplan model over our temperature range. Quasiparticle recombination in the Ti/Al stack following a nontypical law suggests that other mechanisms rather than pure BCS recombination set the practical sensitivity of the detector. Our analysis using two different phenomenological models (i.e., the modified Arrhenius form and a power law) reproduce the measured data. The first indicates that an effective activation energy below Δ_0 is in play (since the phenomenological parameter m is lower than one), while the second points that electron–phonon processes dominate the quasiparticle dynamics in the system. Both phenomenological models provide comparably good fits to the measured recombination times over the explored temperature range, indicating that the present data do not allow us to unambiguously discriminate between gap inhomogeneity-driven recombination and phonon-mediated relaxation mechanisms.

Both interpretations are natural in a Ti/Al bilayer. Proximity effects [22] and material inhomogeneities [17] can produce subgap states that dominate the GR kinetics, yielding an apparent $m < 1$ in the modified Arrhenius model. On the other hand, the quasiparticle dynamics can be influenced also from phonon processes like, for example, phonon trapping or diffusion bottlenecks originated in thermal phonons that cannot dissipate due to acoustic mismatch between layers [23], [24]. These phonon processes tend to steepen the temperature dependence toward T^{-n} with $n \sim 4$. In our case, gap inhomogeneity and phonon transport dominate the GR dynamics, following previous studies based on disordered superconductors like TiN [17]. Future measurements under controlled illumination may shade light on this subject.

Combining measured responsivities with the noise spectra, we determine a minimum dark electrical NEP of $\sim 3 \times 10^{-19}\,\mathrm{W}\sqrt{\mathrm{Hz}}$ at 200 Hz and $T_{\rm bath} = 100$ mK, which sets a lower bound on the optical NEP for these devices. We propose different engineering strategies that can be implemented to improve the NEP value, as follows:

1) using membranes or phononic structures as substrate can enhance phonon escape and suppress rebreaking, improving responsivity and, thus, the NEP value [15], [25];
2) reducing the volume of the absorber to increase responsivity [26];
3) improving thermalization in our set-up will also improve phonon dissipation, avoiding quasiparticle poisoning from phonon diffusion mechanisms.

V. Conclusion

The presented results constitute a complete study of the superconducting electrodynamics of Ti/Al LEKID aimed at axion search and astrophysical observations in the W-band (75–110 GHz). Using an MB analysis, we obtained a thermal

equilibrium description of the Ti/Al bilayer, consistent with the measured T_c and EM estimations, confirming suitability across the full W-band. From phase-noise spectroscopy, we find that quasiparticle recombination kinetics deviate from BCS prediction; in contrast, the data are well captured by phenomenological models, pointing to gap inhomogeneity and phonon diffusion bottlenecks as dominant nonequilibrium processes.

In summary, these results establish a starting point for the development of dark matter axion detectors based on Ti/Al LEKIDs. The developed prototype has achieved competitive sensitivity under dark conditions. Although the measured NEP sets a lower bound, it still remains uncertain whether the observed deviation from the expected BCS recombination dynamics will affect the optical NEP. Future work will address this question through dedicated experiments under controlled illumination.

ACKNOWLEDGMENT

The authors would like to thank R. Ferrándiz from INTA (Spain) for his support designing and fabricating the chip holder. They also would like to thank also the CADEx Collaboration for useful discussions.

REFERENCES

[1] R. Adam et al., "The NIKA2 large-field-of-view millimetre continuum camera for the 30 m IRAM telescope," *Astron. Astrophys.*, vol. 609, 2018, Art. no. A115.
[2] P. Ade et al., "A wide field-of-view low-resolution spectrometer at apex: Instrument design and scientific forecast," *Astron. Astrophys.*, vol. 642 2020, Art. no. A60.
[3] A. Endo et al., "Wideband on-chip terahertz spectrometer based on a superconducting filterbank," *J. Astron. Telesc. Instrum. Syst.*, vol. 5, no. 3, 2019, Art. no. 035004.
[4] J. Glenn et al., "PRIMA: The probe far-infrared mission for astrophysics," *Proc. SPIE*, vol. 13092, 2024, Art. no. 130920J.
[5] B. Aja et al., "The Canfranc axion detection experiment (CADEx): Search for axions at 90 Ghz with kinetic inductance detectors," *J. Cosmol. Astroparticle Phys.*, vol. 2022, no. 11, Nov. 2022, Art. no. 044.
[6] J. Zmuidzinas, "Thermal noise and correlations in photon detection," *Appl. Opt.*, vol. 42, no. 25, pp. 4989–5008, Sep. 2003.
[7] V. Rollano et al., "Cross-polarization reduction in kinetic inductance detectors based on quasi-lumped resonators," *IEEE Trans. Microw. Theory Techn.*, vol. 74, no. 1, pp. 449–456, Jan. 2026.
[8] A. Catalano et al., "Bi-layer kinetic inductance detectors for space observations between 80–120 GHz," *Astron. Astrophys.*, vol. 580, 2015, Art. no. A15.
[9] S. Probst, F. Song, P. A. Bushev, A. V. Ustinov, and M. Weides, "Efficient and robust analysis of complex scattering data under noise in microwave resonators," *Rev. Sci. Instrum.*, vol. 86, 2015, Art. no. 024706.
[10] J. Gao, "The physics of superconducting microwave resonators," Ph.D. dissertation, California Institute of Technology, Pasadena, CA, USA, 2008.
[11] J. Gao, J. Zmuidzinas, A. Vayonakis, P. Day, B. Mazin, and H. Leduc, "Equivalence of the effects on the complex conductivity of superconductor due to temperature change and external pair breaking," *J. Low Temp. Phys.*, vol. 151, no. 1, pp. 557–563, 2008.
[12] Sonnet Software Inc., "Sonnet em," 2024. [Online]. Available: https://www.sonnetsoftware.com/
[13] P. J. de Visser, J. Baselmans, J. Bueno, N. Llombart, and T. Klapwijk, "Fluctuations in the electron system of a superconductor exposed to a photon flux," *Nature Commun.*, vol. 5, no. 1, 2014, Art. no. 3130.
[14] S. B. Kaplan, C. Chi, D. Langenberg, J.-J. Chang, S. Jafarey, and D. Scalapino, "Quasiparticle and phonon lifetimes in superconductors," *Phys. Rev. B*, vol. 14, no. 11, 1976, Art. no. 4854.
[15] S. A. De Rooij, J. J. Baselmans, V. Murugesan, D. J. Thoen, and P. J. De Visser, "Strong reduction of quasiparticle fluctuations in a superconductor due to decoupling of the quasiparticle number and lifetime," *Phys. Rev. B*, vol. 104, no. 18, 2021, Art. no. L180506.
[16] J. Gao et al., "A titanium-nitride near-infrared kinetic inductance photon-counting detector and its anomalous electrodynamics," *Appl. Phys. Lett.*, vol. 101, no. 14, 2012, Art. no. 142602.
[17] J. Bueno et al., "Anomalous response of superconducting titanium nitride resonators to terahertz radiation," *Appl. Phys. Lett.*, vol. 105, no. 19, 2014, Art. no. 192601.
[18] A. Sergeev and V. Mitin, "Electron-phonon interaction in disordered conductors: Static and vibrating scattering potentials," *Phys. Rev. B*, vol. 61, no. 9, 2000, Art. no. 6041.
[19] A. Kardakova et al., "The electron-phonon relaxation time in thin superconducting titanium nitride films," *Appl. Phys. Lett.*, vol. 103, no. 25, 2013, Art. no. 252602.
[20] M. Sidorova et al., "Electron energy relaxation in disordered superconducting NbN films," *Phys. Rev. B*, vol. 102, no. 5, 2020, Art. no. 054501.
[21] S. Zhao, D. J. Goldie, S. Withington, and C. N. Thomas, "Exploring the performance of thin-film superconducting multilayers as kinetic inductance detectors for low-frequency detection," *Supercond. Sci. Technol.*, vol. 31, no. 1, 2017, Art. no. 015007.
[22] A. Hosseinkhani and G. Catelani, "Proximity effect in normal-metal quasiparticle traps," *Phys. Rev. B*, vol. 97, no. 5, 2018, Art. no. 054513.
[23] S. B. Kaplan, "Acoustic matching of superconducting films to substrates," *J. Low Temp. Phys.*, vol. 37, no. 3, pp. 343–365, 1979.
[24] K. Rostem, P. De Visser, and E. Wollack, "Enhanced quasiparticle lifetime in a superconductor by selective blocking of recombination phonons with a phononic crystal," *Phys. Rev. B*, vol. 98, no. 1, 2018, Art. no. 014522.
[25] P. J. De Visser, S. A. De Rooij, V. Murugesan, D. J. Thoen, and J. J. Baselmans, "Phonon-trapping-enhanced energy resolution in superconducting single-photon detectors," *Phys. Rev. Appl.*, vol. 16, no. 3, 2021, Art. no. 034051.
[26] S. A. de Rooij, J. J. Baselmans, J. Bueno, V. Murugesan, D. J. Thoen, and P. J. de Visser, "Volume dependence of microwave-induced excess quasiparticles in superconducting resonators," *Phys. Rev. Appl.*, vol. 24, no. 2, 2025, Art. no. 024007.

Victor Rollano received the B.Sc. and M.Sc. degrees in physics from the Universidad Complutense de Madrid, Madrid, Spain, 2014 and 2015, respectively, and the Ph.D. degree in superconducting vortex dynamics on reconfigurable potentials from the Universidad Complutense de Madrid and IMDEA Nanoscience, Madrid, Spain, in 2019.

His doctoral research focused on the dynamics of superconducting vortices in engineered pinning landscapes created by magnetic and superconducting nanostructures. From 2020 to 2021, he was a Postdoctoral Researcher with the Quantum Materials and Devices Group, Instituto de Nanociencia y Materiales de Aragón (CSIC), Zaragoza, Spain, where he contributed to the development of quantum processing units based on molecular spins. He is currently with the Centro de Astrobiología (CSIC-INTA), Madrid, Spain, where his work focuses on the development of kinetic inductance detectors for dark matter detection experiments.

Dr. Rollano was the recipient of the Margarita Salas Fellowship in 2021 and the Marie Skłodowska-Curie Fellowship in 2022 to pursue research on hybrid quantum devices combining nitrogen-vacancy ensembles in diamond with superconducting qubits, carried out with the Hybrid Quantum Devices Group, University of Science and Technology of China (USTC), Hefei, China.

Alejandro Pascual Laguna was born in Madrid, Spain, in 1992. He received the B.Sc. degree in telecommunications engineering from ICAI School of Engineering, Universidad Pontificia Comillas, Madrid, Spain, in 2014 after spending an exchange year from the Chalmers University of Technology, Gothenburg, Sweden, and the M.Sc. (*cum laude*) and the Ph.D. degrees in electrical engineering from the Delft University of Technology, Delft, The Netherlands, in 2016 and 2022, respectively.

From 2016 to 2023, he was with Space Research Organization of the Netherlands, Leiden, The Netherlands, first as a Ph.D. candidate and then as a Scientist. From 2023, he is with CAB, the Astrobiology Center (CSIC-INTA), Torrejón de Ardoz, Spain, where he is currently a Juan de la Cierva fellow. His research interests include on-chip solutions for efficient broadband (sub)millimeter wavelength imaging spectrometers and polarimeters based on ultra-sensitive kinetic inductance detectors.

David Rodriguez was born in Zamora, Spain, in 1996. He received the B.Sc. degree in physics and the M.Sc. degree in condensed matter physics from the Universidad Autónoma de Madrid, Madrid, Spain, in 2018 and 2019, respectively. He is currently working toward the Ph.D. degree in the field of superconducting circuits for quantum technologies and quantum sensing with the Centro de Astrobiología (CSIC-INTA), Madrid, Spain, under the supervision of Alicia Gómez.

During his B.Sc. degree, he joined the Department of Condensed Matter Physics, Universidad Autónoma de Madrid as a Research Assistant where he was involved in quantum transport measurements. He later joined the Advanced Nanomaterials and Devices, Technical University of Einhoven, Eindhoven, The Netherlands, to conduct his master's thesis. In 2021, he joined Alicia Gomez's group as a Research Assistant and later become a Ph.D. student. He is also involved in the development and control of qubits in collaboration with INMA-Universidad de Zaragoza, Zaragoza, Spain. His research focuses on the design of superconducting resonators for quantum and space applications.

Martino Calvo received the Graduate and Ph.D. degrees from the University of Rome Sapienza, Rome, Italy, in 2005 and 2009, respectively. His Ph.D. dissertation was titled "Development of the first Lumped Element KIDs Dedicated to Millimeter Wave Detection."

He continued his work on KIDs during a 2 years Postdoc grant with the same university, before moving to France where he joined the Néel Institute, CNRS Grenoble, Grenoble, France, in 2011. Since then, he has been involved in the development and realization of various instruments for mm-wave astronomy, in particular NIKA2, the first KID-based camera to observe the sky, and CONCERTO, a wide Field-of-View spectrometer that has been deployed with the APEX Telescope, Antofagasta, Chile, from 2021 to 2023. He has been a Research Engineer with Néel Institute, since 2016.

Maria Teresa Magaz was born in Madrid, Spain, in 1965. She received the B.Sc. and M.Sc. degrees in organic chemistry from Universidad Autónoma de Madrid, Madrid, Spain, 1986 and 1988, respectively, and the M.Sc. degree in occupational health and safety in 2010.

She was a Research Assistant Technician with La Marañosa, Institute of Technology (INTA), Madrid, Spain, from 2010 to 2015, working on optical photolithography for the development of PbSe IR detectors. Since 2017, she has been a Research Assistant Technician with Centro de Astrobiología (CSIC-INTA) in collaboration with IMDEA-Nanociencia, Madrid, Spain. Her research focuses on processing and optimization of nano and microfabrication of ultrasensitive detectors for astronomy and quantum technologies. Her expertise includes sputtering and e-beam evaporation deposition in high vacuum conditions, dielectric deposition using Atomic Layer Deposition (ALD), optical and electrical lithography, wet and dry etching techniques, and fabrication characterization.

Daniel Granados received the Ph.D. degree in physical sciences from the Autonomous University of Madrid (UAM), Madrid, Spain, in 2006.

He is currently the Executive Director of Scientific Infrastructures with the Madrilenian Institute for Advanced Studies in Nanoscience (IMDEA Nano) and head of the Quantum NanoDevices Group. He is also a Physicist. He completed his experimental doctoral studies at the Institute of Microelectronics in Madrid, which is a part of the National Microelectronics Center, Spanish National Research Council (IMN-CNM-CSIC), Madrid, Spain. For three years, he was a Researcher with the Quantum Information Group, Toshiba Research Europe Ltd., Cambridge, U.K., and the leader of the Photonic Confinement Group. He joined IMDEA-Nano in 2009 as the head and coordinator of nanofabrication services.

Dr. Granados is the vice-president of the Electronic Materials division of the International Union for Vacuum Science, Technique, and Applications (IUVSTA) and a member of the scientific advisory committee of the Spanish Vacuum Association (ASEVA). Since 2021, he has been a member of the Executive Committee of the Circle Foundation for Security and Defense Technologies. Since 2022, he has also been a Scientific/Technical Advisor to the General Directorate for Research and Technological Innovation of the Community of Madrid for the PERTE-CHIP, and a member of the expert committee of the Think Tank Future Trends Forum of the Bankinter Innovation Foundation. He contributed to the creation and launch of the Madrid Cluster for Innovation, Technology, and Talent in Semiconductors of the Community of Madrid and has been its Director since January 2023.

Alessandro Monfardini received the master's degree in space physics and the Ph.D. degree in nuclear physics from the University of Milano and Instituto Nazionale di Fisica Nucleare, Milano, Italy, in 2000.

He is a Physicist. He is currently a Research Director with CNRS - Institut Néel - Grenoble, Grenoble, France. He has developed instrumentation for Astrophysics, Particles, and Nuclear Physics. He has worked in Italy, Japan, U.K., and France.

Alicia Gomez received the Ph.D. degree in physics, with a focus on superconducting vortex dynamics, from the Universidad Complutense de Madrid, Madrid, Spain, in 2013.

Since then, she has led the Superconducting Technologies Group, Centro de Astrobiología (CSIC-INTA), Madrid, Spain, working on the development of kinetic inductance detectors (KIDs) for astrophysical instrumentation in space and ground-based observatories. Her expertise ranges from the design and nanofabrication of superconducting devices to their cryogenic characterization. She has participated in major international collaborations, including the NIKA2 Camera installed at the IRAM 30 m telescope, Granada, Spain, the KISS Camera for the Canary Islands telescope, and the CORE proposal. She is currently leading the development of KIDs for the CADEx experiment dedicated to the search for dark matter. More recently, her research has expanded to the design of optimized superconducting circuits for implementation in proof-of-concept large-scale molecular spin quantum processors. She has also been a visiting Researcher with the University of California, Davis, CA, USA, the University of Antwerp, Antwerp, Belgium, and the Institut Néel, Grenoble, France.